



Observational aspects of outbursting black hole sources: Evolution of spectro-temporal features and X-ray variability

H. SREEHARI^{1,2,*} , ANUJ NANDI¹, D. RADHIKA³, NIRMAL IYER⁴ and SAMIR MANDAL⁵

¹Space Astronomy Group, ISITE Campus, ISRO Satellite Centre, Outer Ring Road, Marathahalli, Bengaluru 560 037, India.

²Department of Physics, Indian Institute of Science, Bengaluru 560 012, India.

³Department of Physics, Dayananda Sagar University, Bengaluru 560 068, India.

⁴Albanova University Centre, KTH PAP, Stockholm 10691, Sweden.

⁵Department of Physics, Indian Institute of Space Science and Technology, Thiruvananthapuram 695 547, India.

*Corresponding author. E-mail: hjsreehari@gmail.com

MS received 2 September 2017; accepted 1 January 2018; published online 9 February 2018

Abstract. We report on our attempt to understand the outbursting profile of Galactic Black Hole sources, keeping in mind the evolution of temporal and spectral features during the outburst. We present results of evolution of quasi-periodic oscillations, spectral states and possible connection with jet ejections during the outburst phase. Further, we attempt to connect the observed X-ray variabilities (i.e., ‘class’/‘structured’ variabilities, similar to GRS 1915+105) with spectral states of black hole sources. Towards these studies, we consider three black hole sources that have undergone single (XTE J1859+226), a few (IGR J17091-3624) and many (GX 339-4) outbursts since the start of *RXTE* era. Finally, we model the broadband energy spectra (3–150 keV) of different spectral states using *RXTE* and *NuSTAR* observations. Results are discussed in the context of two-component advective flow model, while constraining the mass of the three black hole sources.

Keywords. Accretion—X-ray binaries—black holes—ISM: jets and outflows—radiation mechanisms.

1. Introduction

A Galactic Black Hole (GBH) binary system consists of a primary black hole and a secondary star. If the secondary star is a Sun-like star with mass of a few solar masses, it is called a Low Mass X-ray Binary (LMXB) and if the companion star is a few tens of solar masses in size, it is a High Mass X-ray Binary (HMXB). The primary accretes matter from the secondary star via Roche lobe over flow in the case of LMXBs and from stellar winds in the case of HMXBs. A few X-ray binaries also have intermediate mass companions and such systems are termed as Intermediate Mass X-ray Binaries (IMXBs) (Podsiadlowski *et al.* 2002).

Tetarenko *et al.* (2016) reported 77 GBH sources while Corral-Santana *et al.* (2015) reported 59 transient GBH sources, of which 18 are dynamically confirmed. Till date, three extragalactic black hole transients also have been observed. They are LMC X-1, LMC X-3 and

M33 X-7 (see Corral-Santana *et al.* 2015 for details). Besides these, we also have Ultra-Luminous X-ray sources (ULXs) which may harbour intermediate mass black holes (Feng & Soria 2011). GBH systems can be either persistent or outbursting (Tanaka & Shibazaki 1996). Some GBHs like Cyg X-1 show persistent X-ray emission while some others like GRS 1915+105 are persistent with aperiodic variability. Sources like GX 339-4 undergo frequent outbursts separated by quiescent states. There are also sources like GRO J1655-40 that remain mostly in the quiescent state and goes into outburst once in a decade or so.

During an outburst a typical black hole binary system goes through different canonical states (Homan & Belloni 2005; Belloni *et al.* 2005; Remillard & McClintock 2006; Nandi *et al.* 2012). These are the Low Hard State (LHS), Hard Intermediate State (HIMS), Soft Inter-Mediate State (SIMS) and the High Soft State (HSS). It is the mass transfer rate onto the BH

which determines the transient behaviour of the source (Tanaka & Lewin 1995). During the LHS, the source energy spectrum can be modelled mainly with a *powerlaw* component along with a *gaussian* (for the iron line) and reflection components. The presence of a disk is usually seen as the system undergoes transition into the intermediate states and the disk contribution increases significantly as the source enters the HSS. Meanwhile, the *powerlaw* index also increases from around 1.5 in the LHS to values as high as 2.8 in the HSS.

One can study the state evolution of black hole binaries using the outburst profile as well as the ‘q-diagram’ or Hardness Intensity Diagram (HID). The HID of a typical outburst is a hysteresis loop in the shape of a ‘q’ (Homan & Belloni 2005). From the HID, it is evident that the decay phase of the outburst always has lower total flux values as compared to the rising phase.

As the system evolves through different states we also see variation in its temporal characteristics. Specifically, we see different types of Quasi-Periodic Oscillations (QPOs) in the power spectrum of the source. Low-Frequency QPOs (LFQPOs) are generally found in the LHS, HIMS and SIMS. They are categorized into Type A, Type B and Type C based on the frequency of oscillation, rms value, quality factor and significance. Casella *et al.* (2004) gave a detailed classification of LFQPOs. A few black hole binary systems also exhibit High Frequency QPOs (HFQPOs). But in this paper, we restrict our study only to C-Type LFQPOs as they show evolution in their frequencies during the rising and decay phases of an outburst.

Black Hole Binaries (BHBs) also exhibit different types of variability in their light curves. Some sources like GRS 1915+105 are known to exhibit structured ‘class’ variability. Apart from X-ray outbursts and variabilities in smaller time scales, BHBs are also observed to exhibit bipolar radio jet emissions (Fender *et al.* 2004).

1.1 Motivation and source selection

The motivation of this work is to do a comparative study of the outburst profiles, QPO evolution and X-ray spectral evolution of three black hole binary sources namely XTE J1859+226, GX 339-4 and IGR J17091-3624. These three sources have also shown signature of X-ray variability during their outbursts. We compare these variability with the structured variability exhibited by the source GRS 1915+105.

XTE J1859+226 has gone into an outburst only in 1999 following which it has been in quiescence. GX

339-4 is one of the most active transient sources which has undergone several outbursts in the RXTE-SWIFT era. Meanwhile, IGR J17091-3624 undergoes an outburst approximately once in every four years since its discovery in 2003. Hence we have chosen these three BHBs which differ in their frequency of outbursts. Figure 1 shows the frequency of outbursts of four different sources.

Besides this all three sources have shown evolution of low-frequency QPOs and we could model them with the Propagating Oscillatory Shock (POS) model. Also we have done spectral modelling of the four different states of the black hole binary GX 339-4 using the two-component advective flow model. For this, we have chosen only the 2002 outburst of GX 339-4 as a sample. The modelling with phenomenological models as well as the two-component flow for the hard and soft states of the other two sources (XTE J1859+226 and IGR J17091-3624) are also shown in this paper. Estimation of mass of the black holes in these sources are also done using the two-component flow model. Detailed modelling of the entire outbursts of these two sources is going on and will be published elsewhere. We have also compared the variability exhibited by the three sources we consider with that exhibited by GRS 1915+105.

We also intend to study the possible connection between X-ray variability and state classification of the sources thereby interpreting the state of GRS 1915+105. This is done based on the states of the three BHBs (XTE J1859+226, GX 339-4 and IGR J17091-3624) during the period in which they exhibit variability.

2. Observation, analysis and modelling

We have considered the observations of different black hole binaries carried out with the All-Sky Monitor (ASM), Proportional Counter Array (PCA) and the High Energy X-ray Timing Experiment (HEXTE) aboard the satellite Rossi X-ray Timing Explorer (RXTE). The ASM is operated in the energy range of 1.3 keV to 12.2 keV and we obtain the outburst profile of various sources using this instrument. PCA data in the energy range of 2 to 60 keV and HEXTE data in 15 to 200 keV were usually considered for spectral studies. We extract the energy spectrum from PCA and HEXTE using standard techniques. The PCA data is used for both spectral and temporal analysis while HEXTE is used mainly for generating energy spectrum at higher energies. Broadband energy spectrum combining PCA and HEXTE is modelled to study the state evolution of different black hole binary systems.

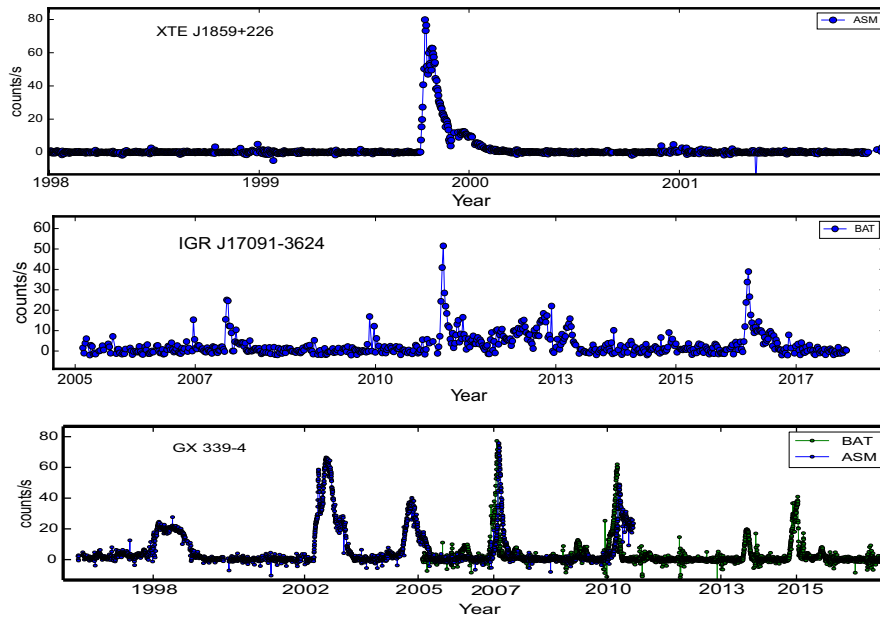


Figure 1. Light curve of some outbursting GBHs showing that the frequency of outburst varies from source to source. XTE J1859+226 has had only one outburst in the last two decades. GX 339-4 goes into outburst once in every two or three years while IGR J17091-3624 clearly shows outbursts in 2007, 2011 and 2016.

Besides the spectral studies, we also search PCA data for the presence of peaked noise components or QPOs. The science event files are used to extract the light curves which are used to generate the power spectrum. We model the obtained power spectra with *powerlaws* and/or *Lorentzians*. If any QPO-like feature is found then it is fit with *Lorentzians*. The significance of QPOs in the spectrum are calculated as the ratio of norm to its negative error. If significance > 3 and the quality factor, $Q = \nu/\text{FWHM}$ is found to be greater than 2 then the narrow feature is considered as a QPO. QPOs are classified into low-frequency QPOs (LFQPOs) and high-frequency QPOs (HFQPOs) based on their frequency ranges. Typically LFQPOs appear in the frequency range of 0.1 to 30 Hz and HFQPOs appear at frequencies more than 30 Hz and extends up to ≈ 500 Hz in the case of black hole binaries. The highest HFQPO observed so far in black hole binaries is from the source GRO J1655-40 and it is 450 Hz (Strohmayer 2001).

We also analysed *SWIFT-XRT* data of IGR J17091-3624 and studied the variability of the source. *XRT* operates in the range from 0.5 to 10 keV. *xrtpipeline* was run to obtain cleaned event files which were then filtered corresponding to grades 0–2 using *XSELECT* software. We chose a circular region of 30 arc seconds centred at the source RA and DEC to obtain the source region and an annular region of 60 arc second inner radius and 90 arc second outer radius as the background region (see

Radhika *et al.* 2016b for further details). Then we extract light curves and energy spectra corresponding to these source and background regions. The background subtracted light curves are then used to produce the power spectra for further analysis. We use *xrtmkarf* to generate the *arf* files and then we re-bin the extracted source energy spectra to 25 counts per bin with the *ftool grp-pha*.

Six TOO observations with NuSTAR are also available for the 2016 outburst of IGR J17091-3624. We include spectral studies based on two of those (from LHS and SIMS) in this paper. The other four broadband spectra are studied in detail by Radhika *et al.* (2017). We use *nupipeline* to extract the level 2 data based on the procedure given in the NuSTAR guide¹. A circular region of 30'' centred at the source RA and DEC is used as the source region and another 30'' circle far away from the source is taken as the background region. Then we use the *ftool nuproducts* to extract the spectrum, response and *arf* files. The obtained spectrum is re-binned to 30 counts per bin. In the next section, we present the results of the data analysis done with the three sources under consideration.

¹<https://heasarc.gsfc.nasa.gov/docs/nustar/analysis/nustarswguide.pdf>.

3. Results: spectro-temporal features of outbursting BH sources

In order to study the spectro-temporal features of outbursting BH sources, we consider three sources XTE J1859+226, GX 339-4 and IGR J17091-3624. The X-ray transient source XTE J1859+226 was discovered with ASM onboard RXTE on October 9, 1999 (Wood *et al.* 1999). Detailed studies of the outburst had revealed the spectral state characteristics of the source (Homan & Belloni 2005; Radhika & Nandi 2014). GX 339-4 is a well-known transient source and has undergone several outbursts during the *RXTE-SWIFT* era (see Fig. 1). Detailed study of its spectral and temporal evolution have paved the way for understanding the general characteristics of GBH transients (Motta *et al.* 2011; Nandi *et al.* 2012). The source IGR J17091–3624 was discovered by the International Gamma-Ray Astrophysics Laboratory (INTEGRAL) in the year 2003 and also did exhibit multiple outbursts. A very detailed study of the source has revealed its spectral and temporal properties (Capitanio *et al.* 2006, 2012; Iyer *et al.* 2015). The most significant feature of the source is the variabilities/oscillations discovered in its light curve during the 2011 outburst (Altamirano *et al.* 2011). These have been found to be similar to the well-known source GRS 1915+105 (Belloni *et al.* 2001). In the following subsections we will discuss the outburst profile, QPO evolution, state evolution, jet connection, X-ray variability and broad band spectral modelling of black hole binary sources.

3.1 Outburst profile

Outbursting black hole sources either have a Fast Rise Exponential Decay (FRED) or a Slow Rise Exponential Decay (SRED) profile. In Fig. 2, we present a typical FRED outburst profile and the corresponding q-diagram exhibited by the microquasar XTE J1859+226 in the year 1999. The q-diagram or the Hardness Intensity diagram (HID) is the plot of total flux versus hardness ratio (ratio of flux in higher energy range to that in the lower energy range). Black hole binaries (BHB) undergo state transitions from hard to soft state as the outburst progresses. Hard states correspond to observations with considerable amount of high energy photons while the soft states will be dominated by thermal emission with minimum contribution from high energy photons. A typical black hole binary outburst will go through different spectral states (see for details, Homan *et al.* 2001; Belloni *et al.* 2005; Remillard & McClintock 2006;

Nandi *et al.* 2012) during the outburst. The outburst profile and q-diagram for XTE J1859+226 is shown in Fig. 2. We chose the outburst of XTE J1859+226 as it is a good representative for the outburst and q-profiles for BHBs. It evolves through all the canonical states and hence we have included only this profile in the paper. Similar plots for GX 339-4 and IGR J17091-3624 will be presented elsewhere.

As the outburst begins, the source is in LHS where the hardness ratio is maximum. This is followed by the HIMS where the photon counts are high and there is significant contribution from the higher energies. The source then enters the SIMS where the hardness ratio reduces and the soft flux increases. When in the HSS the hardness ratio reaches its minimum value and the spectrum is dominated by thermal emission. In the declining phase the source again occupies the SIMS, HIMS and LHS with similar values for the hardness ratio as was the case for the rising phase. In Fig. 2, we show the rising phase LHS in blue patch, HIMS in yellow patch, SIMS in orange patch and HSS in red patch. After the HSS the source enters the decay phase. The decay phase characteristics are similar to that of the corresponding states in the rising phase except for a decrease in total flux values. We also note that during the LHS and HIMS of both rising and decay phases, LFQPOs are detected. They generally evolve from around 0.1 Hz to a maximum of around 20 to 30 Hz. Here we study the LFQPO evolution in the rising phase.

3.2 Evolution of LFQPOs

Outbursting black hole sources exhibit QPOs which are features that peak in the power spectrum generated from source light curves. Typically LFQPOs are of three types C, B and A (Casella *et al.* 2004). C type LFQPOs appear in the LHS and HIMS only. A and B types are of lesser rms values and are seen in the SIMS. C-type QPOs appear in power spectra with flat top while the A and B QPOs are found where the power spectra exhibits weak power-law noise. In this paper, we study C-type QPOs, as unlike A and B QPOs they increase in frequency during the rising phase of an outburst and decrease in frequency during the decay phase of the outburst.

As mentioned above C-type LFQPOs show a time evolution and can be considered to have origins based on shock propagation. The Propagating Oscillatory Shock (POS) model (Chakrabarti *et al.* 2005, 2008; Iyer *et al.* 2015) explains the time evolution of C-type QPOs as a function of shock location. The shock location is essentially the size of the post-shock corona region around

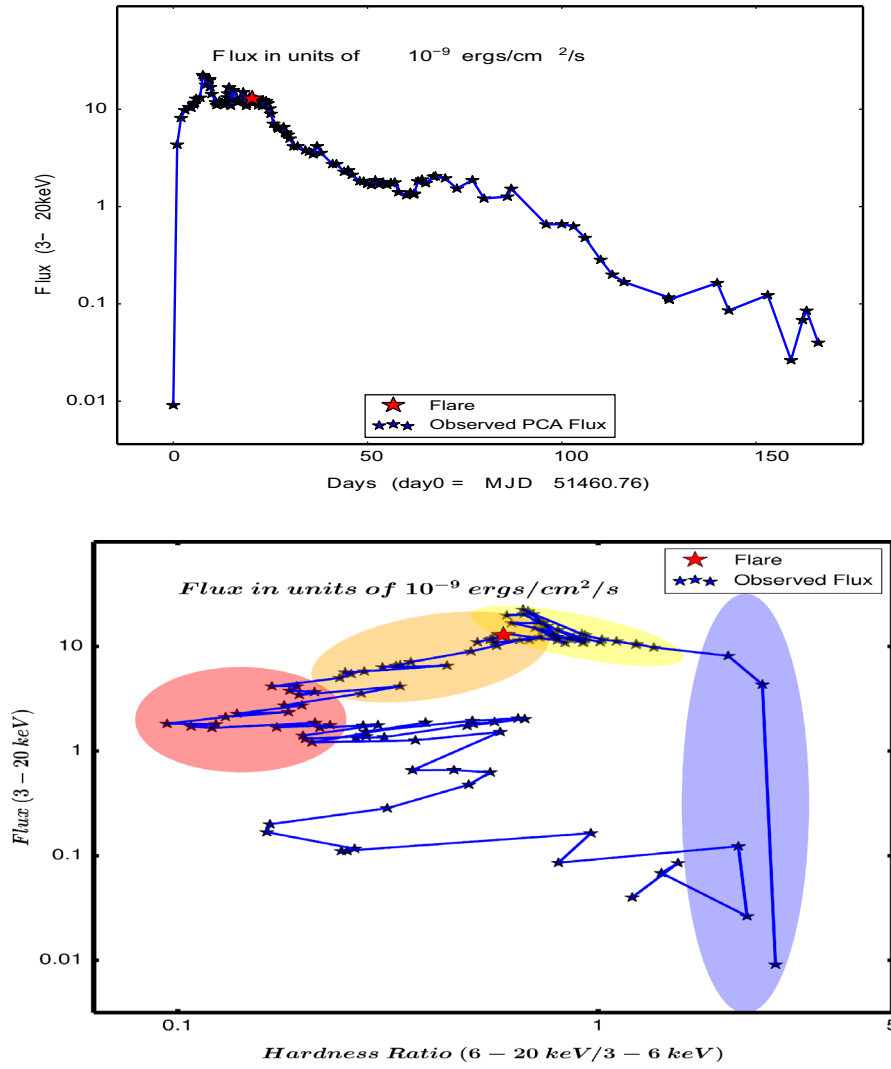


Figure 2. The *top panel* gives the outburst profile of the source XTE J1859+226 during its 1999 outburst. It is a typical FRED profile with the rising phase extending only around 30 days while the decay phase is gradual and takes more than 140 days. The red marker corresponds to a radio flare observed during this outburst. The corresponding q-plot is shown in the *bottom panel*. The blue stars indicate the observed flux versus hardness ratio. The rising phase states are marked in coloured patches. The LHS is shown in blue patch, HIMS in yellow patch, SIMS in orange patch and HSS in red patch. We also show the occurrence of a radio flare in both the outburst profile and the HID using a red color star.

the black hole. The model considers that QPOs are generated by the oscillation of this region. POS model is given by

$$\nu_{\text{qpo}} = \frac{c}{2\pi R r_g r_s \sqrt{r_s - 1}}$$

and

$$r_s = r_{\text{so}} - \frac{vt + \frac{at^2}{2}}{r_g},$$

where ν_{qpo} is the QPO frequency, R is the shock compression ratio or shock strength, v is the velocity of the shock front, a is the acceleration, r_s is the instantaneous

shock location and r_{so} is the initial shock location given in units of $r_g = \frac{2GM}{c^2}$.

This model implicitly depends on mass of the compact object and hence can be used to estimate the black hole mass from the time evolution of QPOs. Typically the time evolution of QPOs are smooth without any discontinuity. In Fig. 3, we show the case for XTE J1859+226 during its 1999 outburst. Here we see that initially the QPO frequency increases with time, and then breaks and halts for a while. It then proceeds again with a smooth variation. The two frequencies in the shaded region of Fig. 3 corresponding to the days MJD 51464.10 and MJD 51464.63 are identical as well as

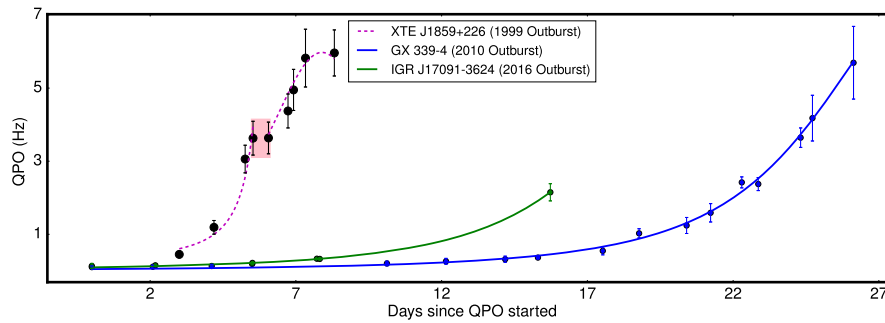


Figure 3. The QPO evolution of XTE J1859+226 during its 1999 outburst, GX 339-4 during its 2010 outburst and IGR J17091-3624 during its 2016 outburst are shown. The shaded region shows a QPO frequency which did not evolve for around half a day.

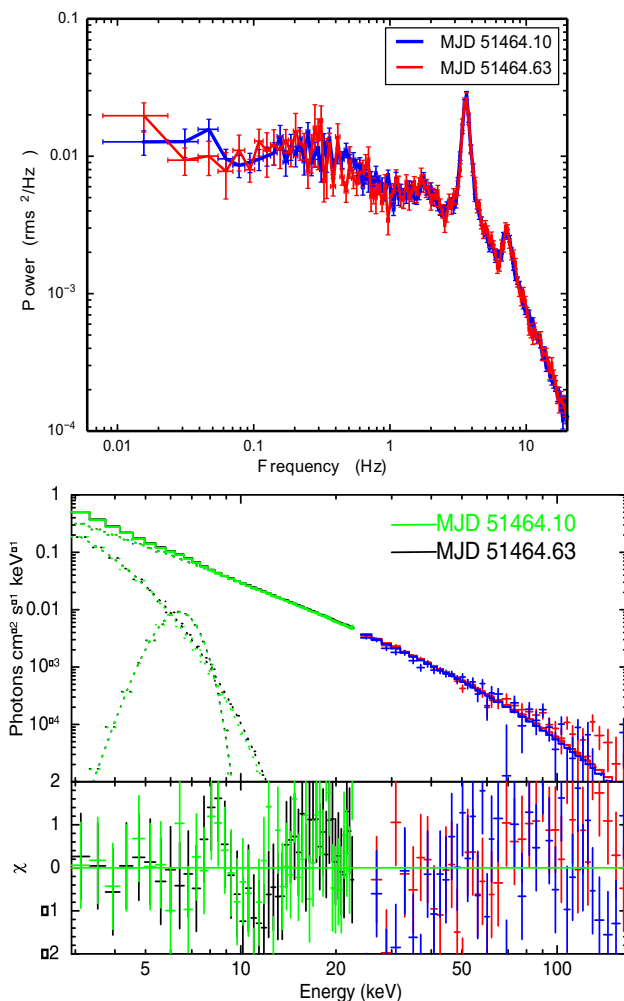


Figure 4. The power spectra (*top panel*) and the energy spectra (*bottom panel*) of the observations corresponding to the shaded region in Fig. 3 are plotted here. The green and blue lines respectively indicate the PCA and HEXTE spectrum on MJD 51464.10 while the black and red lines correspond to the observation on MJD 51464.63. It is evident that the system did not evolve during this period as both energy spectra and power spectra are almost identical.

their power spectra are overlapping as is shown in Fig. 4. From here, we infer that the QPO parameters like its frequency, width, normalization and rms are also identical during this period. Examining the energy spectra corresponding to the two observations shaded in pink, we find that the spectral parameters are also identical in this period. This suggests that the accretion process has been steady and has not evolved from this state for a while. Besides this, the QPO evolution for this outburst started off with an offset of 3 days as was required for the curve fitting using POS model. This indicates that the QPO evolution has started off earlier, but we do not have the data as the source was not observed in that period. The other two C-type LFQPO evolutions in Fig. 3 correspond to GX 339-4 (2010 outburst) and IGR J17091-3624 (2016 outburst). This shows that QPO evolution for different outbursts extends for different durations. The QPO evolution of XTE J1859+226 is steep while that for GX 339-4 is gradual. Also we notice that in the case of IGR J17091-3624 the maximum frequency reached only till 2.1 Hz while for the other two sources the maximum frequency reached around 6 Hz.

The results of POS modelling for the three sources are presented in Table 1. For XTE J1859+226, modelling its QPO evolution gave a shock location of $206 r_g$, initial acceleration of $7.4219 \times 10^{-06} \text{ m/s}^2$ followed by a deceleration of $1.6021 \times 10^{-05} \text{ m/s}^2$ after the halt and a mass of $5.35 \pm 0.9 M_\odot$. Here the modelling is different from Radhika and Nandi (2014) where they considered two POS fits for the two sections of QPO evolution before and after the halt and no acceleration was used. For the source GX 339-4, 2010 outburst, the shock velocity is $10.73 \pm 2 \text{ m/s}$, constant deceleration is $1.4527 \times 10^{-06} \text{ m/s}^2$, the initial shock location is $437 r_g$ and the estimated mass is $10.65 \pm 1.67 M_\odot$. For the source IGR J17091-3624, we obtained an initial shock

Table 1. Fit parameters from the POS model.

Source	Outburst	Mass (M_{\odot})	x_s (r_g)	Initial velocity (m/s)	Acceleration (m/s^2)
XTE J1859+226	1999	5.35 ± 0.9	206	0 ± 0.10	$7.42 \times 10^{-06}, -1.60 \times 10^{-05}$
GX 339-4	2010	10.65 ± 1.67	437	10.73 ± 2	-1.45×10^{-06}
IGR J17091-3624	2016	11.08 ± 0.79	297	9.93 ± 1.39	-1.80×10^{-06}

location of $297r_g$, initial velocity of 9.93 ± 1.39 m/s, a constant deceleration of $1.8077 \times 10^{-06} m/s^2$ and mass of $11.08 \pm 0.79M_{\odot}$. Now we will discuss about the different spectral states that the black hole binary sources go through during their outburst phase.

3.3 Spectral state evolution

Outbursting sources transit through different states as was introduced earlier. The spectral evolution of the source XTE J1859+226 has been observed to be similar to typical GBH binaries. The spectra could be modelled using disk and *powerlaw* components. The source occupied all the spectral states of LHS, HIMS, SIMS and a short duration of HSS, and did complete the q-profile in its HID (see Fig. 2). The temporal properties revealed the presence of type A, B, C and C* (in decay phase) QPOs. A detailed study on this source have been discussed in Radhika and Nandi (2014).

The energy spectra from the LHS and HSS of XTE J1859+226 has been shown in Fig. 5. The PCA (RXTE) energy spectral data is plotted in black while the HEXTE (RXTE) spectral data is plotted in red. The dotted lines indicate the contribution from components used in the model like *diskbb* and *powerlaw*. For the LHS, we fitted with the model *phabs(smedge*cutoffpl)*. The smeared edge was at 7.16 keV and the high energy cut-off was at 50 keV. The photon index of the spectrum was 1.61 ± 0.04 . For the HSS, we required a *diskbb* at 0.75 keV and a *powerlaw* with index 2.39 ± 0.18 . The HSS spectrum extended only till 25 keV and no cut-off was required.

We have modelled the energy spectrum of the source GX 339-4 as it went through the LHS, HIMS, SIMS and HSS in its 2002 outburst. It was observed that the spectra could be modelled with a *powerlaw* alone for the hard states while we required an additional disk component (*diskbb*) to model the hard intermediate and soft states. The power law index, Γ for the LHS was 1.58 which corresponds to a flat spectrum. For HIMS and SIMS, the photon index was 2.51 and 2.52 respectively and for HSS, it was $\Gamma = 2.18$. Though the value of Γ is lower than expected for HSS, it should be noted that

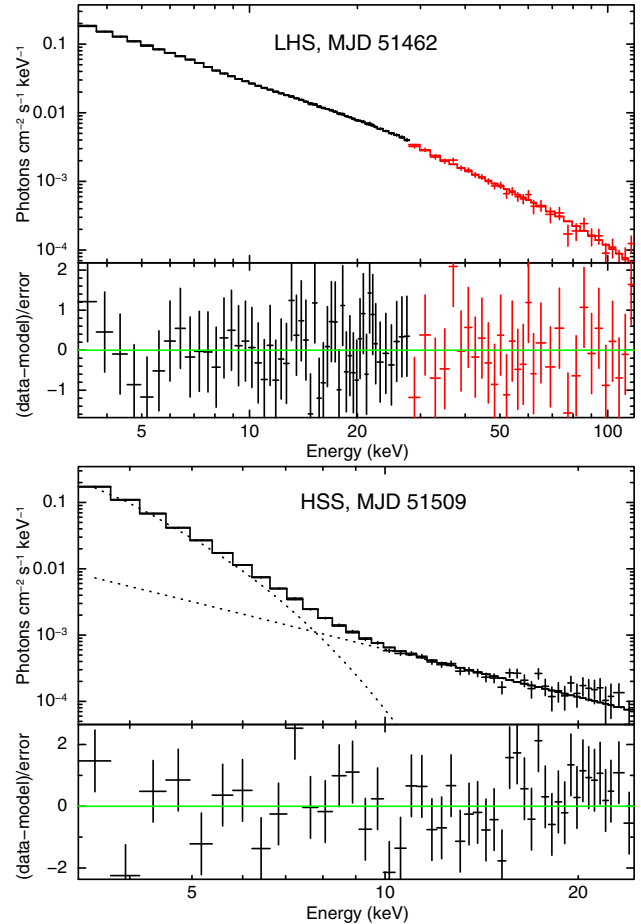


Figure 5. Phenomenological modelling of RXTE (PCA-HEXTE) spectra in LHS and HSS of the source XTE J1859+226 during its 1999 outburst. The black lines are spectral data from RXTE-PCA and the red lines are data from the RXTE-HEXTE instrument.

the percentage contribution of the total flux by *diskbb* in this state was 76.47%. The presence of *diskbb* in the model indicates a significant contribution of the multi-temperature black body emission with an inner disk temperature of 0.60 keV and confirms that the source is in HSS. Figure 6 shows the phenomenological modelling of all four states of the source GX 339-4 during its 2002 outburst observed by *RXTE*.

IGR J17091-3624 during its 2016 outburst was found to occupy the LHS, HIMS and SIMS and only a very

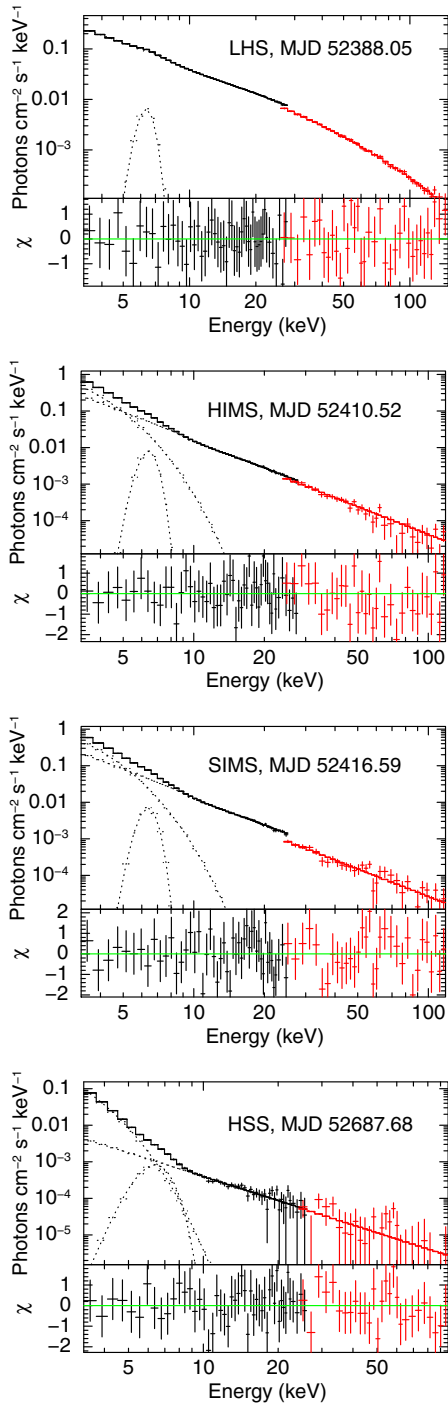


Figure 6. Phenomenological modelling of energy spectra corresponding to the four states LHS, HIMS, SIMS and HSS of GX 339-4 during its 2002 outburst. The black curves are from RXTE–PCA (3–25 keV) and the red curves are from RXTE–HEXTE (25–150 keV). The dotted lines indicate the contribution from model components like *diskbb*, *gaussian* and *powerlaw*.

short presence of HSS (lasting for only a day) (Radhika *et al.* 2017). We have included two energy spectra from the 2016 outburst of this source corresponding to the

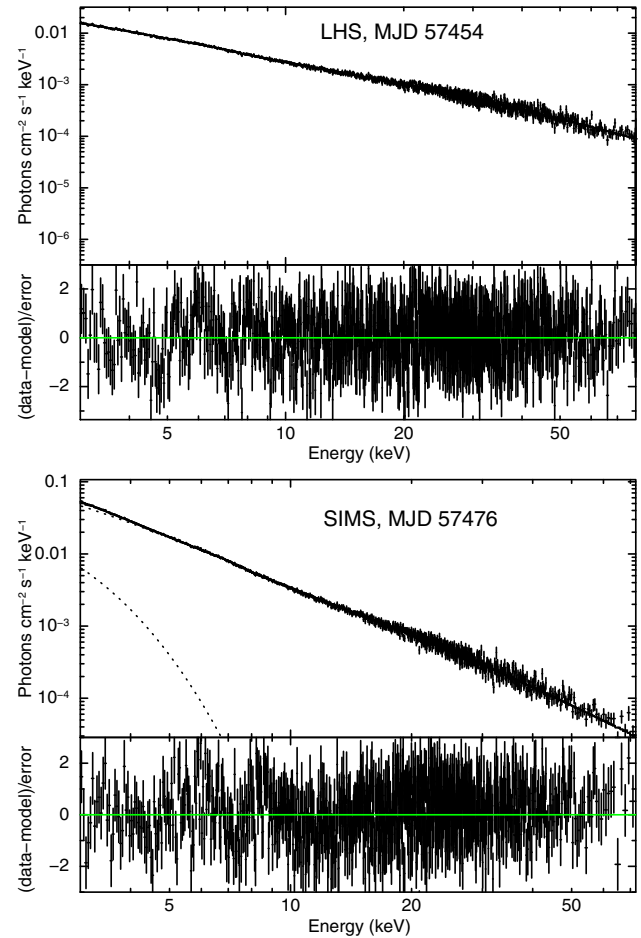


Figure 7. Phenomenological modelling of NuSTAR spectra in LHS and SIMS of the source IGR J17091-3624 during its 2016 outburst. The general model used for fitting is $phabs(diskbb + ireflect * cutoffpl)$.

LHS and SIMS in Fig. 7. These are isolated NuSTAR observations. The energy spectra of IGR J17091-3624 was modelled using *disk*, *ireflect* and *cutoffpl* components. We obtained a relative reflection value of 0.39 ± 0.04 and 0.60 ± 0.05 for LHS and SIMS respectively. The photon index for LHS was 1.58 ± 0.01 and for the SIMS it was 2.41 ± 0.02 . The analysis of simultaneous XRT–NuSTAR observations and details of the full outburst (2016) including state classification, variability and mass estimation will appear in Radhika *et al.* (2017).

3.4 Connection between QPO, spectral states and jet ejection

Radio jets are a very common phenomena in the black hole accretion process. During ‘soft’ X-ray states, the radio emission is strongly suppressed while jets are observed during the ‘hard’ states (Fender *et al.* 2004,

2009). The relativistic jets are observed as the system changes states from HIMS to SIMS. As an example we have shown the case of the source XTE J1859+226 during its 1999 outburst in Fig. 2 with the location of one of its radio flares marked in red. For a detailed study on the flares from this source, see Radhika and Nandi (2014).

We observed that QPOs are absent during the period of multiple jet ejections or flaring of the source XTE J1859+226 (Radhika & Nandi 2014; Radhika *et al.* 2016a) have shown that type CLFQPOs appear around a day before the jet ejection. There is no presence of QPOs when the flare occurs, while type B QPOs are observed a few hours later. During flares, there is no phase lag observed between the soft and hard photons. When comparing the flux contributions it has been observed that disk flux dominates over the non-thermal flux during flares. In the LHS and HIMS, the type C QPO frequency increases as both the disk and powerlaw flux increases. In the rising phase as well as in the declining phase of the outburst, strong radio jets have been observed. During the SIMS, it was found that the type B QPO frequency is correlated with powerlaw flux, but not with disk flux. This indicates that type B QPOs originate from the corona. It has also been noted that a few of the type C QPOs in SIMS are not correlated with the powerlaw flux while all C* QPOs are correlated only with the disk flux. Besides this the power density spectra had very low rms during the flare.

Similarly in GX 339-4 during the 2002 and 2010 outbursts, absence of QPOs have been found during the time a radio flare was detected (Radhika *et al.* 2016a). The correlation of radio flux with X-ray flux for the source GX 339-4 has been studied in detail by Corbel *et al.* 2013. Due to lack of radio observations of IGR J17091-3624 during its outbursts, we could not explore this characteristic of disk-jet coupling.

3.5 X-ray variability

Next, we look into the variability exhibited by the three sources that we are studying. Here we additionally use GRS 1915+105 as a reference source as it is known for its class variabilities. Figure 8 shows the variability exhibited by the sources GRS 1915+105 (in 1997), IGR J17091-3624 (in 2016), XTE J1859+226 (in 1999) and GX 339-4 (in 2002, 2007 and 2010). Belloni *et al.* (2001) gave a detailed analysis of the different classes of variability expressed by the source GRS 1915+105. We have shown in Fig. 8 the ρ , κ and θ class variabilities of GRS 1915+105. Thus we see variability at different time scales (50 s, 100 s and 600 s) for GRS 1915+105.

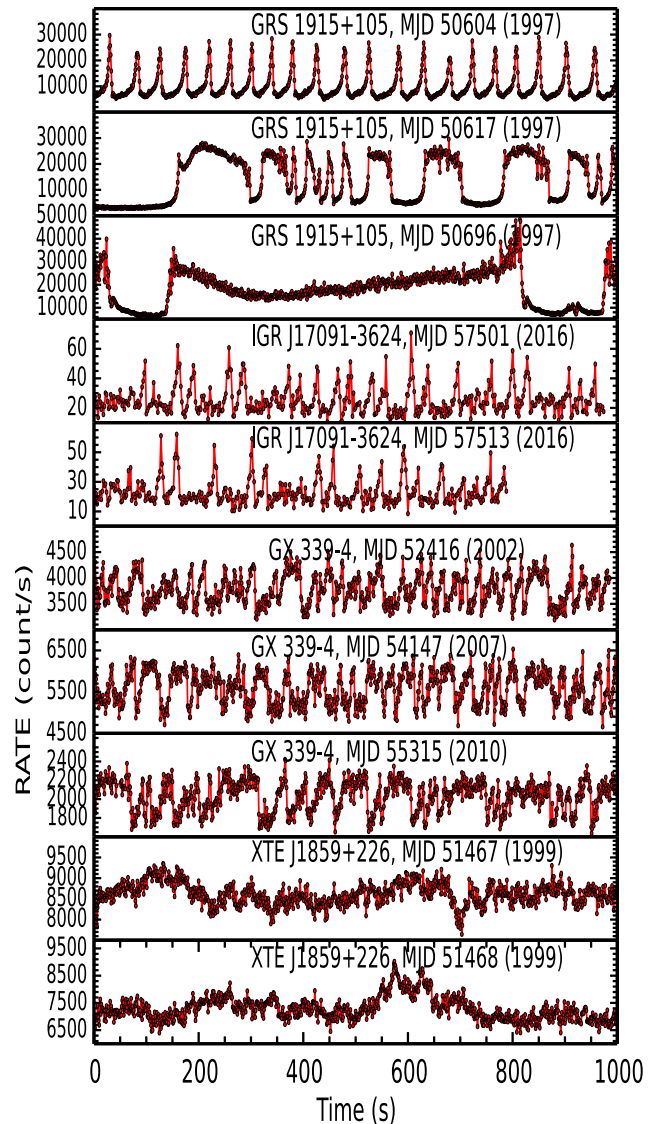


Figure 8. Structured variability exhibited by different sources during their outbursts. The first three panels show three of the variabilities exhibited by GRS 1915+105 corresponding to ρ , κ and θ classes respectively. The remaining panels compare it with the variabilities of IGR J17091-3624 (2016), GX 339-4 (2002, 2007 and 2010) and XTE J1859+226 (1999). The variabilities exhibited by the latter three sources were during the period of SIMS which gives us reasonable evidence that GRS 1915+105 must also be in one of its intermediate states.

We compare it with the light curves of other sources and find that XTE J1859+226 does not have a well-defined structure in its light curves while IGR J17091-3624 and GX 339-4 show some structure or repetitions in their light curves. The GX 339-4 light curves showing variability has flat tops separated by flat bottoms. It may be a combination of the ρ and κ classes exhibited by GRS 1915+105.

We did not find any signature of variabilities during the LHS and HIMS. During the SIMS, we observed that the IGR J17091-3624 exhibits variabilities in the light curve (Radhika *et al.* 2017) similar to that expressed by the same source in its 2011 outburst (Capitanio *et al.* 2012; Iyer *et al.* 2015). In HSS also the system showed oscillations, though weaker than that during the SIMS. It is noticed that IGR J17091-3624 is very faint as compared to the other sources that we study. Similarly in XTE J1859+226 and GX 339-4, we find signatures of variabilities when the source has transited to the SIMS.

It is also observed that for these sources the variability is observed only in light curves corresponding to the intermediate spectral states. Thus we infer that possibly GRS 1915+105 must also be in one of its intermediate states as it shows structured variability during these observations.

4. Broadband spectral modelling with two-component flow: mass estimation

The two component advective flow (Chakrabarti & Titarchuk 1995; Chakrabarti & Mandal 2006; Iyer *et al.* 2015) model incorporates a Keplerian disk (Shakura & Sunyaev 1973) as well as a sub-Keplerian halo around the black hole. The Keplerian disk is in the equatorial region and the sub-Keplerian halo is on the top and bottom sides of the disk. During the hard states the sub-Keplerian component predominates the flux contribution while during the soft states the major flux contribution is from the Keplerian disk. Here unlike in phenomenological models, the high and low energy photon emission are dependent on each other. As the outburst progresses the effect of the sub-Keplerian component reduces and the disk starts contributing more to the total flux of the source.

We self-consistently calculate the total radiation spectrum from hydrodynamics (Mandal & Chakrabarti 2005) and import the two-component advective flow model as an additive table in *XSPEC* (Iyer *et al.* 2015). For each source under consideration there are four variable parameters in this model. They are the mass of the black hole (M_{BH}) in units of M_{\odot} , shock location (r_s) in units of r_g , Keplerian disk accretion rate, \dot{m}_d and sub-Keplerian halo accretion rate (\dot{m}_h) in units of Eddington rate. Besides this we have the *norm* parameter which is a constant for a source as it is dependent on distance to the source, its mass and inclination. For the fitting we use spectra from 3 to 150 keV. During the softer states as the higher energy range of the spectral data decreases, we fit only up to 80 keV or so. We

Table 2. Spectral fit parameters using phenomenological and two component flow models.

Source	MJD (state)	Observatory	T _{in} (keV)	rel _{refl}	Photon index	High-cut (keV)	\dot{m}_h, \dot{m}_d (\dot{M}_{Edd})	Mass (M_{\odot})	x_s (r_g)	Two component flow parameters	
										Phenomenological parameters	Two component flow parameters
XTE J1859+226	51462 (LHS)	PCA-HEXTE	—	—	1.61 ± 0.04	50 ± 8.0	0.26, 0.15	6.0 ± 0.053	101 ± 2		
XTE J1859+226	51509 (HSS)	PCA	0.75 ± 0.005	—	2.39 ± 0.18	—	0.18, 0.49	6.05 ± 0.27	24.6 ± 1.2		
GX 339-4	52388 (LHS)	PCA-HEXTE	—	0.39 ± 0.17	1.58 ± 0.04	71 ± 6	0.20, 0.04	11.56 ± 0.17	424 ± 7		
GX 339-4	52410 (HIMS)	PCA-HEXTE	0.86 ± 0.01	—	2.52 ± 0.02	—	0.06, 3.3	11.02 ± 0.14	190 ± 12		
GX 339-4	52416 (SIMS)	PCA-HEXTE	0.88 ± 0.03	—	2.51 ± 0.07	—	0.04, 0.57	10.21 ± 0.35	46 ± 2		
GX 339-4	52687 (HSS)	PCA-HEXTE	0.60 ± 0.05	—	2.18 ± 0.11	—	0.64, 10.6	9.55 ± 0.47	5 ± 0.03		
IGR J17091-3624	57454 (LHS)	NuSTAR	—	$0.39^{+0.06}_{-0.06}$	$1.58^{+0.028}_{-0.028}$	228^{+72}_{-44}	0.36, 0.04	11.66 ± 0.12	484 ± 18		
IGR J17091-3624	57476 (SIMS)	NuSTAR	$0.59^{+0.014}_{-0.015}$	$0.60^{+0.07}_{-0.08}$	$2.41^{+0.017}_{-0.020}$	—	0.07, 0.19	11.51 ± 0.07	56 ± 2		

perform fitting with the two-component model for all data sets of an outburst of the source leaving the norm parameter free. Then we take an average of all the norms and fix it as the norm for the source. The fit results for both phenomenological and two-component models for all three sources under consideration are presented in Table 2.

Figure 9 shows the energy spectra of the source XTE J1859+226 during its 1999 outburst modelled using the two-component flow. We are including only two states (LHS and HSS) in this paper. Detailed analysis of each state of the outburst is presented in Nandi *et al.* (2017). When the source was in the LHS (on MJD 51462), it had a halo accretion rate of $0.26\dot{M}_{\text{Edd}}$ and a Keplerian accretion rate of $0.15\dot{M}_{\text{Edd}}$. The shock location was at $101 \pm 2r_g$ and the mass of the source is estimated as $6.0 \pm 0.53M_{\odot}$. In the HSS, the accretion rates are $0.18\dot{M}_{\text{Edd}}$ for the halo and $0.49\dot{M}_{\text{Edd}}$ for the disk. The computation of shock location gave a value of $24.6 \pm 1.2r_g$. The mass estimate for the source from this model is $6.05 \pm 0.27M_{\odot}$.

In Fig. 10, we have shown the two-component flow based on spectral modelling performed for GX 339-4 during its 2002 outburst. Here, we find that during the LHS the shock location is $424 \pm 7r_g$, the halo rate is $0.20\dot{M}_{\text{Edd}}$ and the disk rate is $0.04\dot{M}_{\text{Edd}}$. As the source moves to HIMS, the shock location becomes $190 \pm 12r_g$. The halo rate declines to $0.06\dot{M}_{\text{Edd}}$ while the disk rate increases to $3.3\dot{M}_{\text{Edd}}$. In SIMS, the shock location has reduced further to $46 \pm 2r_g$, the halo rate is $0.04\dot{M}_{\text{Edd}}$ and the disk rate increased to $0.57\dot{M}_{\text{Edd}}$. Finally in the HSS, we obtained the limiting value of the shock location of $5r_g$, a halo rate of 0.64 and a disk rate of 10.6 both in units of \dot{M}_{Edd} . We also estimated the mass from spectral modeling with two-component flow and found that GX 339-4 mass lies in the range 9.20 to $11.95M_{\odot}$. Heida *et al.* (2017) estimated the black hole mass of GX 339-4 to be between $2.3M_{\odot}$ and $9.5M_{\odot}$. Detailed broadband spectral modelling of all outbursts of GX 339-4 is under progress and the results will be presented elsewhere.

Similarly, we have studied the source IGR J17091-3624 during its 2016 outburst by means of two-component flow modelling of SWIFT and NuSTAR simultaneous spectra (Radhika *et al.* 2017). During the LHS the shock location obtained was $484r_g$ and it reduced to $56r_g$ as the source entered the SIMS. The halo accretion rate changed from 0.36 to $0.07\dot{M}_{\text{Edd}}$ and the disk accretion rate increased from 0.04 to $0.19\dot{M}_{\text{Edd}}$. The mass estimates from the two observations included in this paper are 11.66 ± 0.12 and $11.51 \pm 0.07M_{\odot}$.

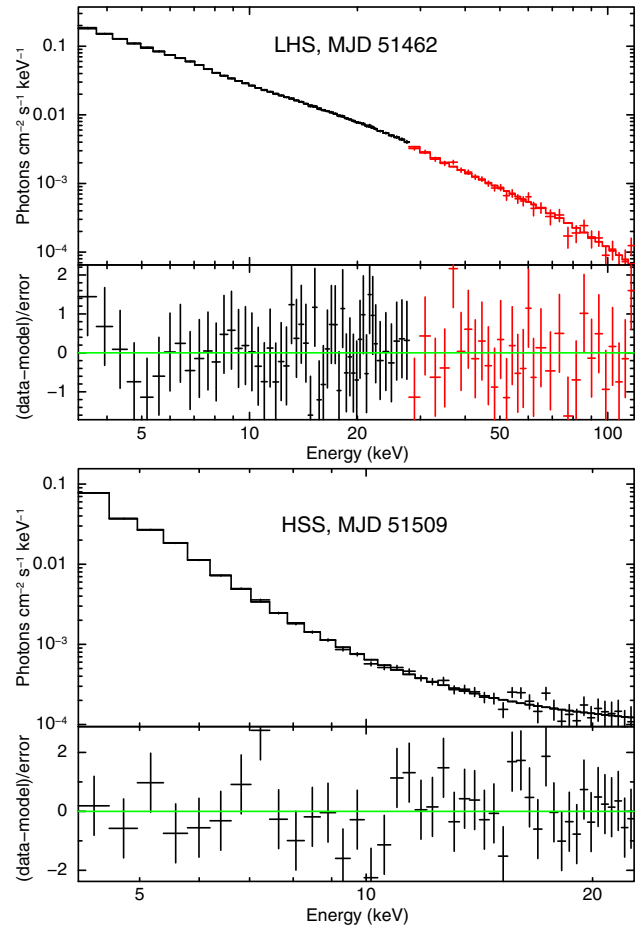


Figure 9. Two-component flow modelling of RXTE (PCA-HEXTE) spectra in LHS and HSS of the source XTE J1859+226 during its 1999 outburst.

Figure 11 shows the energy spectra of IGR J17091-3624 during the LHS and SIMS of its 2016 outburst as observed by NuSTAR. Thus we could understand the spectral evolution of the different sources based on both phenomenological and two-component advective flow modelling and estimate the mass of the compact objects in these systems.

5. Conclusion and future work

In this paper, we show the evolution of spectro-temporal characteristics of three different GBH binaries. First, we saw that the frequency of outbursts for different sources are different. Some sources like GX 339-4 are dynamic whereas sources like XTE J1859+226 remain in a quiescent phase for most of the time. The light curve evolution of these sources show that they do not have a unique variation of the intensity. The light curves are found to be either a FRED or slow rise and exponential decay.

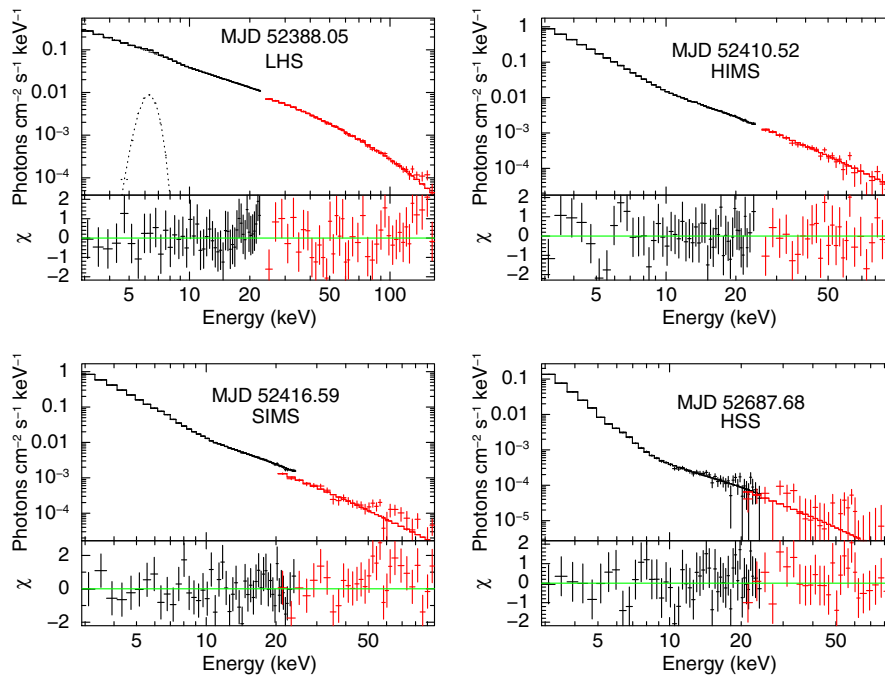


Figure 10. Two component flow modelling of energy spectra corresponding to the four states of GX 339-4 during its 2002 outburst. The black lines correspond to spectral data from PCA, the red lines correspond to spectral data from HEXTE and the dotted lines are the model components like *gaussian* and two-component flow.

We have studied how the black hole binary sources evolve along the hardness intensity diagram (q-plot) during their outburst. The sources XTE J1859+226 and GX 339-4 are observed to complete the q-profile and hence exhibit all the spectral states. IGR J17091-3624 is found to be different from this typical variation and do not occupy all the spectral states. The 2016 outburst of IGR J17091-3624 has just one observation corresponding to a possible HSS wherein the hardness ratio was a minimum and the signature of the disk was prominent (Radhika *et al.* 2017).

We have also modelled the energy spectra using the two-component model and found the variation of spectral characteristics to be matching with that obtained using phenomenological modelling. With the help of this, we have been able to find that the shock location decreases as a source evolves from its LHS to HSS. Additionally, the variation of halo rate and disk rate agrees well with the variation of soft and hard fluxes respectively. During the LHS, the halo rate is found to be maximum and decreases as the source approaches HSS. Similarly the disk rate increases when the source energy spectra softens towards the HSS (Radhika *et al.* 2017).

The temporal characteristics show the presence of LFQPOs in the power spectra. Different types like A, B, C and C* have been identified for the different sources. The C type QPO frequency is observed to increase as

the outburst progresses. We also modelled the time evolution with the help of the POS model and understand that the QPO is generated by the propagation of a shock front (see Fig. 3).

There also exists a possible connection between the occurrence of radio flares and spectro-temporal characteristics of the sources. Figure 2 shows the location of radio flare for the 1999 outburst of the source XTE J1859+226. We find that during the period the flare occurs as indicated by radio light curves, the power spectra does not show the presence of QPOs and the total rms variability decreases (Radhika & Nandi 2014). The energy spectra is observed to get softer as is evident in the increase of soft flux (disk rate) and decline in the hardness ratio. This suggests that probably the innermost part of the disk (hot corona) is being evacuated into jets/flares, resulting in the soft flux to dominate. Hence the absence of any oscillations of the corona leads to no detection of QPOs. Thus we can be certain that the origin of QPOs is linked with the oscillations of the corona.

An interesting feature observed in all the sources studied in this paper, is the occurrence of variability signatures in the X-ray light curves. These are found to be similar to that observed in GRS 1915+105 (Belloni *et al.* 2001) and IGR J17091-3624 (2011 outburst; Altamirano *et al.* 2011). We find that the variability signatures are not identical for all the sources studied here.

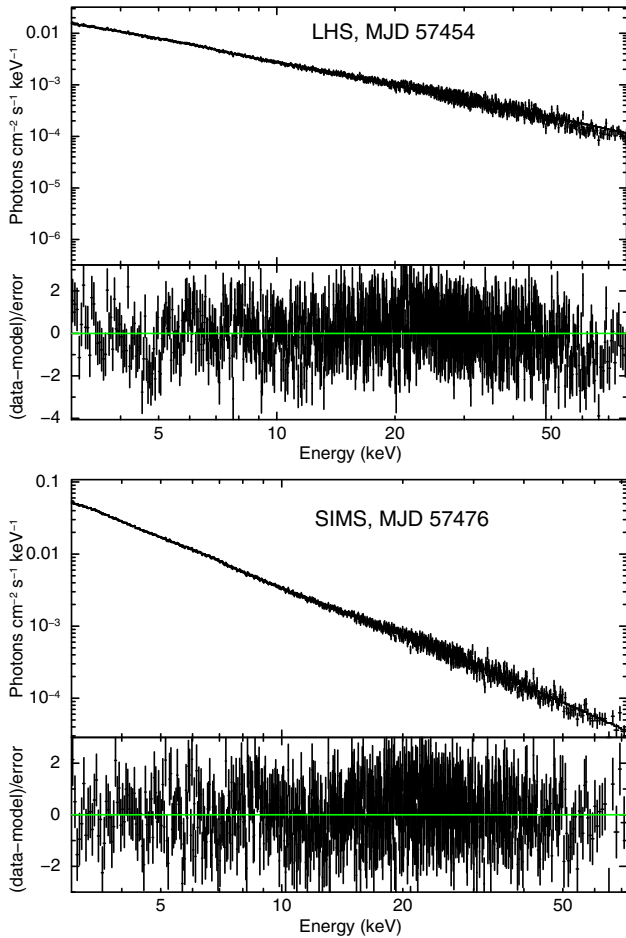


Figure 11. Two-component flow modelling of NuSTAR spectra in LHS and SIMS of the source IGR J17091-3624 during its 2016 outburst.

Additionally, a comparative study with the spectral evolution suggest that these variabilities appear at the time the source transits to the intermediate state (specifically SIMS in XTE J1859+226 and GX 339-4). We consider this as an indication that GRS 1915+105 which exhibits different class variabilities is also in one of the intermediate states.

Finally, we also modelled the energy spectra of the three sources using the two-component advective flow paradigm and estimated the Keplerian and sub-Keplerian accretion rates, shock location and mass of the compact object. These results are presented in Table 2.

In this paper, we have not considered the effects of black hole spin in order to understand the spectro-temporal evolution. As a future study, we intend to do the analysis of QPOs and jet ejection mechanisms in the Kerr space. Broadband analysis and modelling of the energy spectra considering the rotational effects of the compact object can shed new light on the origin of

QPOs. Moreover, the effect of black hole spin on the flaring of the BHBs will also be studied in detail.

Acknowledgements

The authors are thankful to the reviewer whose valuable suggestions have helped in improving the manuscript. AN thanks GD, SAG; DD, PDMSA and Director, ISAC for encouragement and continuous support to carry out this research. This research has made use of the data obtained through High Energy Astrophysics Science Archive Research Center online service, provided by NASA/Goddard Space Flight Center.

References

Altamirano D., Belloni T., Linares M., van der Klis M., Wijnands R., Curran P. A., Kalamkar M. *et al.* 2011, *Astrophys. J. Lett.*, 742.2, L17

Belloni T., Méndez M., Sánchez-Fernández C. 2001, *A&A*, 372, 551

Belloni T., Homan J., Casella P., Van Der Klis M., Nespoli El., Lewin W. H. G., Miller J. M., Méndez M. 2005, *A&A*, 440-1, 207

Capitanio F., Bazzano A., Ubertini P., Zdziarski A. A., Bird A. J., De Cesare G., Dean A. J., Stephen J. B., Tarana A. 2006, *ApJ*, 643, 376

Capitanio F., Del Santo M., Bozzo E., Ferrigno C., De Cesare G., Paizis A. 2012, *MNRAS*, 422, 3130

Casella P., Belloni T., Homan J., Stella L. 2004, *A&A*, 426-2, 587

Corbel S., Coriat M., Brocksopp C., Tzioumis A. K., Fender R. P., Tomsick J. A., Buxton M. M., Bailyn C. D. 2013, *MNRAS*, 428, 2500

Corral-Santana J. M., Casares J., Munoz-Darias T., Bauer F. B., Martinez-Pais I. G., Russell D. M. 2016 *A&A*, 587, A61

Chakrabarti S. K., Mandal S. 2006, *Astrophys. J. Lett.*, 642, L49

Chakrabarti S. K., Titarchuk L. G. 1995, *ApJ*, 455, 623

Chakrabarti S. K., Nandi A., Debnath D., Sarkar R., Datta B. G. 2005, *Indian J. Phys.*, 79-8, 841

Chakrabarti S. K., Debnath D., Nandi A., Pal P. S. 2008, *A&A*, 489-3, L41

Fender R. P., Belloni, T. M., Gallo E. 2004, *MNRAS*, 355(4), 1105

Fender R. P., Homan J., Belloni T. M. 2009, *MNRAS*, 396, 1370

Feng H., Soria R. 2011, *New Astron. Rev.*, 55.5, 166

Heida M., Jonker P. G., Torres M. A. P., Chiavassa A. 2017, *ApJ*, 846:132, 8 pp.

Homan J., Wijnands R., Van Der Klis M., Belloni T., van Paradijs J., Klein-Wolt M., Fender R., Mendez M. 2001, *Astrophys. J. Suppl. Ser.*, 132-2, 377

- Homan J., Belloni T. 2005, *Ap&SS*, 300, 107
- Iyer N., Nandi A., Mandal S. 2015, *ApJ*, 807-1, 108
- Motta S., Muñoz-Darias T., Casella P., Belloni T., Homan J. 2011, *MNRAS*, 418, 2292
- Mandal S., Chakrabarti S. K. 2005, *A&A*, 434, 839
- Nandi A., Debnath D., Mandal S., Chakrabarti S. K. 2012, *A&A*, 542, A56
- Nandi A., Mandal S., Sreehari H., Radhika D., Das S., Chattopadhyay I., Iyer N., Agrawal V., Aktar R. 2017, *Ap&SS* (under review)
- Podsiadlowski, Ph., Rappaport, S., Pfahl, E. D. 2002, *ApJ*, 565(2), 1107
- Radhika D., Nandi A. 2014, *Advances in Space Research*, 54-8, 1678
- Radhika D., Nandi A., Agrawal V. K., Seetha, S. 2016, *MNRAS*, 460, 4403
- Radhika D., Nandi A., Agrawal V. K., Mandal S. 2016, *MNRAS*, 462, 1834
- Radhika D., Sreehari H., Nandi A., Iyer N., Mandal, S. 2017, *MNRAS* (under review)
- Remillard R. A., McClintock J. E. 2006, *ARA&A*, 44, 49
- Remillard, R. A., Edward H. M., McClintock J. E., Bailyn C. D., Orosz J. A. 1999, *Astrophys. J.*, 522(1), 397
- Shakura N. I., Sunyaev R. A. 1973, *A&A*, 24, 337
- Strohmer T. E. 2001, *Astrophys. J. Lett.*, 552(1), L49
- Tanaka Y., Lewin W. 1995, in Lewin W., van Paradijs J., van den Heuvel P., eds, *X-ray Binaries*. Press, Cambridge, p. 126
- Tanaka, Y., Noriaki S. 1996, *Ann. Rev. Astron. Astrophys.*, 34(1), 607
- Tetarenko B. E., Sivakoff G. R., Heinke C. O., Gladstone, J. C. 2016, *Astrophys. J. Suppl. Ser.*, 222(2), 15
- Wood A., Smith D. A., Marshall F. E., Swank J. H. 1999, *IAUC*, 7274